

Ti-Al zoning of experimentally grown titanite in the system CaO-Al₂O₃-TiO₂-SiO₂-NaCl-H₂O-(F): Evidence for small-scale fluid heterogeneity

FRIEDRICH LUCASSEN,^{1,2} GERHARD FRANZ,^{1,*} DIETER RHEDE,² AND RICHARD WIRTH²

¹Technische Universität Berlin, Fachgebiet Petrologie, ACK 9, Ackerstrasse 71–76, 13355 Berlin, Germany

²Deutsches GeoForschungsZentrum, Telegrafenberg, 14473 Potsdam, Germany

ABSTRACT

Chemical zoning according to the substitution $\text{Al} + (\text{OH},\text{F}) = \text{Ti} + \text{O}$ is a common phenomenon in natural titanite and can be used to reconstruct its growth conditions. We synthesized titanite, which has a zoning pattern similar to that found in natural titanite that grew at the expense of rutile, visible in element distribution maps as a patchy irregular pattern. Run conditions in the system CaO-Al₂O₃-TiO₂-SiO₂-NaCl-H₂O(-CaF₂) were 600 °C, 0.4 GPa, 1 to 107 days duration. Natural rutile crystals were placed in a perforated Pt-tube within an outer Au-capsule containing wollastonite, γ -Al₂O₃, optionally powdered CaF₂, and a NaCl brine, to simulate conditions, where rutile is transformed into titanite by a hydrous Ca-Si-Al(-F) fluid, driven by a chemical potential gradient between inner and outer capsule. Spontaneous nucleation of titanite is restricted to a small number of crystals on the rutile surface in the inner capsule. Growth proceeds from sparse isolated titanite crystals after 1 day to assemblages of several 100 μm large crystals in a reaction rim in the long-time runs. Titanite is strongly zoned in Al-Ti and shows up to ~ 0.5 Al per formula unit (pfu) in experiments containing F; without F, substitution is limited to ~ 0.25 Al pfu. The range of the Ti-Al exchange is already large in short run times and the same heterogeneity is observed in long-time runs. The Al-Ti distribution (with and without F) in compositional domains (up to several tens of micrometers) is patchy and irregular. No relation of the zoning with time (core-rim) or preferred growth directions was observed.

In the case of fluid-mediated growth, mineral growth zoning represents a disequilibrium at supersaturated conditions. The concentration of Ti in the fluid is likely the limiting factor for titanite growth considering the low solubility compared to that of Al, Ca, and Si. Titanium is not transported in significant amounts into the outer capsule, indicating low mobility, in contrast to Al, Ca, and Si, which are transported into the inner capsule. Assuming buffered Al concentration from dissolution of the Al-source, we speculate that the Ti/Al of the fluid at the precipitation site was controlled by the local Ti concentration, which varies over the distance from the rutile surface to the growing titanite crystal and produces the irregular patchy zoning.

Keywords: Dissolution-precipitation reaction, Al-Ti substitution, mineral zoning, experiments

INTRODUCTION

Titanite (CaTiSiO₅) growth at the expense of rutile (TiO₂) is a common phenomenon during retrogression of granulite, calc-silicate rocks, and eclogite (e.g., Franz and Spear 1985; Lucassen et al. 2010; Gao et al. 2007; Wilke et al. 2010). Typical mineral reactions are grossular + rutile + quartz + H₂O = titanite + zoisite, and grossular + rutile + quartz/coesite = titanite + kyanite, which have been used to constrain *P* and *T* conditions of the titanite formation (e.g., Manning and Bohlen 1991). Titanite-rutile phase relations and stabilities have been investigated experimentally in several early studies, as for example the reaction rutile + calcite + quartz = titanite + CO₂ (e.g., Hunt and Kerrick 1977). More recent studies were concerned with titanite formation in more complex systems including Al and F (e.g., Tropper et al. 2002). The stability field of titanite in comparison with rutile

lies at generally lower *P* and increasing activity of H₂O (e.g., Frost et al. 2000).

Although the solid-solid reactions as listed above are useful and necessary to understand the phase relations in a rock, the actual formation presumably takes place as a fluid-assisted mass transport mechanism of the type rutile + (Ca²⁺+Si⁴⁺)_{fluid} = titanite, as shown by the common occurrence of monomineralic titanite rims on rutile relics and rutile inclusions in titanite (e.g., Lucassen et al. 2010). The driving force for the reaction is the chemical potential gradient between rutile and the rock matrix, which determines the composition of the fluid. A common rock matrix with amphibole and plagioclase (or its high-pressure equivalents) will also contain Al and OH and possibly F, and the titanite-forming reaction can be extended to rutile + (Ca²⁺+Al³⁺+Si⁴⁺±OH,F)_{fluid} = titanite (solid solution).

Major element composition of titanite is dominated by the substitution (Al³⁺,Fe³⁺)+(F⁻,OH⁻) ↔ ^{VI}Ti⁴⁺+O²⁻ (e.g., Oberti et

* E-mail: gerhard.franz@tu-berlin.de

al. 1991). The extent of this substitution (up to 0.5 pfu of Al in natural occurring titanite) has been attributed to variations of the F activity in the fluid phase, the Ti/Al ratio of the chemical environment, and P and T conditions (e.g., Franz and Spear 1985; Enami et al. 1993; Markl and Piazzolo 1999; Castelli and Rubatto 2002; Troitzsch and Ellis 2002; Seifert and Kramer 2003). It was also observed (e.g., Franz and Spear 1985; Lucassen et al. 2010) that Al-Ti zoning is not systematic and although it appears to be growth zoning it cannot be explained in a simple way, such as the classical example of Mn growth zoning in garnet during prograde metamorphism.

The reaction rutile + fluid = titanite provides a simple case, which allows studying some basic principles of a metamorphic mineral reaction, forming a mineral with solid solution around a relict mineral. The purpose of this study is to experimentally investigate titanite growth from rutile in the fluid dominated systems CaO-Al₂O₃-TiO₂-SiO₂-NaCl-H₂O and CaO-Al₂O₃-TiO₂-SiO₂-NaCl-H₂O-F. We used identical P - T conditions of 600 °C and 0.4 GPa, which are near to those for an amphibolite-facies overprint on eclogites or granulites. A NaCl-H₂O or CaF₂-NaCl-H₂O fluid was used to enhance solubility of rutile (Rapp et al. 2010) and to add F to the system. A saline fluid is also typical for metamorphic conditions (e.g., Newton and Manning 2010). Run time was varied from 1 day to ~3 months to get information about reaction progress. We describe variable major element composition and zoning of the titanite overgrowth, as well as the microstructure in the titanite rim, and we conclude that local heterogeneities in the fluid composition are responsible for patchy zoning. Comparisons with natural zoning patterns are given.

EXPERIMENTAL AND ANALYTICAL METHODS

Experimental methods

All experiments were run with similar arrangement of an internal open Pt (2.5 mm outer diameter) and external welded Au capsule (5 mm outer diameter) of maximum 4 cm length (Fig. 1), separating the rutile crystal physically from the other solid starting materials, but leaving a pathway for the fluid. This setup was chosen to simulate the natural conditions where the reaction is fluid mediated. The rutile is a single crystal from a pegmatite in Minas Gerais, Brazil (Table 1) and shows dominantly a combination of (110) and (100) faces, rarely (001) or other faces are preserved in the fragments used for the experiments. It is relatively pure TiO₂ with <1 wt% Fe₂O₃ (Table 1). X-ray powder diffraction analysis (XRD) as well as optical microscopy showed that it is free of other phases such as ilmenite or hematite. Wollastonite is pure CaSiO₃ (Table 1) from a contact metamorphic rock from Namibia. Rutile and wollastonite were cleaned in HNO₃ and HCl, respectively; Au and Pt capsules were boiled in HNO₃. The other ingredients are NaCl, γ -Al₂O₃ and CaF₂ (all analytical grade powders) and distilled H₂O. The bulk composition of wollastonite + γ -Al₂O₃ closely corresponds to that of grossular, and the system is therefore Si-undersaturated, but Al-saturated. Rutile was broken into pieces of approximately 1 mm size with variable weight (Table 2), and one or more grains were placed in the unsealed Pt capsule (Fig. 1). Wollastonite was crushed in an agate mortar to a grain size of <200 μ m. Wollastonite, γ -Al₂O₃ ± CaF₂ (Table 2) were weighed into the Au capsule without homogenizing the respective mixtures. NaCl and H₂O were added in a weight-ratio 1:1 to produce a highly concentrated but not supersaturated fluid at run conditions [$X_{\text{H}_2\text{O}} \sim 0.76$; see Sourirajan and Kennedy (1962), Aranovich and Newton (1996), for the solubility of NaCl]. The activity of H₂O in the pure H₂O-NaCl system is ~0.66 for our run conditions (Aranovich and Newton 1996), but might be further influenced by other cations, Ca, Al, Si, in the solution and by F in the respective compositions. The Pt capsule was placed on top of the mixture and the Au capsule was sealed by arc welding and placed in an oven at 110 °C to check for tightness. The capsules were then placed in externally heated cold-seal vessels, pressurized by water to 0.4 GPa, and heated under controlled pressure to 600 °C. Final temperature was reached after approximately 30 min. The automatic temperature control kept temperature constant within ± 10 °C.

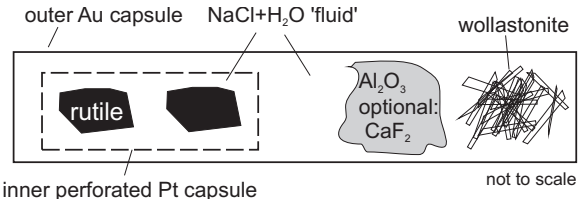


FIGURE 1. Sketch illustrating the experimental setup. The inner Pt-capsule separates the rutile crystals (~1 mm diameter) from the material in the outer Au capsule. The aqueous NaCl-rich fluid is solvent and transport medium for Ca and Si (from wollastonite dissolution), Al and F (by dissolution of γ -Al₂O₃ and CaF₂), and Ti (from rutile dissolution). Two run series, with and without F, were carried out. Not to scale; length of the Au-capsule is ~4 cm.

TABLE 1. Characterization of starting materials; composition given in wt%

Rutile	Wollastonite	γ -Al ₂ O ₃	NaCl	CaF ₂
natural	natural contact	synthetic p.a.	synthetic p.a.	synthetic p.a.
pegmatitic	metamorphic			
Minas Gerais,	Namibia	Merck	Merck	Merck
Brazil		1.01095.100	1.06404.100	2840
TiO ₂ > 98.0	CaO 48.30			
FeO < 1.0	SiO ₂ 51.76			
Nb ~ 0.04–0.2	Al ₂ O ₃ < 0.009			
XRD data				
<i>a</i> 4.59325(6)	<i>a</i> 7.9256(3)			
<i>c</i> 2.59868(8)	<i>b</i> 7.3198(7)			
<i>V</i> 62.422(2)	<i>c</i> 7.0639(2)			
	α 89.968(6)°			
	β 95.216(4)°			
	γ 103.479(7)°			
	<i>V</i> 396.96(4)			

Checks of the pressure during the run time were within the reading precision of ± 10.0 MPa. The vessels were quenched in an air-stream to room temperature within 5 min maintaining the pressure. For the F-free runs the pH of the fluid was measured after the runs by multistep indicator paper and was uniformly 5–6, i.e., within the range at the beginning of the experiments.

Analytical methods

The titanite overgrowth pattern on rutile and the distribution of distinct minerals in the overgrowth was documented by scanning electron microscope (SEM) images. Element mappings were done with SEM on overgrowths on carbon- or gold-coated grain mounts. EMP (electron microprobe) analyses were done using a Cameca SX 100 instrument. Element mapping on polished sections of grain mounts in epoxy resin was carried out in the WDS mode moving the stage in steps of 1–2 μ m, using a beam current of 40–100 nA, and counting times of 300–500 ms per step. Chemical compositions of minerals were determined by wavelength-dispersive X-ray analysis (WDS) techniques. Operating conditions were 15 kV accelerating voltage, 20 nA beam current, and beam diameters of 1–2 μ m. Peak counting times were 10–20 s, backgrounds were counted 5–10 s. Standards used included the following synthetic and natural minerals: topaz (F), albite (Na), orthoclase (Al,Si), boracite (Cl), wollastonite (Ca), rutile (Ti), and hematite (Fe). The raw intensity data were corrected with the PAP program (Pouchou and Pichoir 1988).

Representative run products were investigated by transmission electron microscopy (TEM), using focused ion beam sample preparation (FIB). Electron transparent foils with the typical dimensions $15 \times 10 \times 0.150 \mu\text{m}^3$ were cut from selected areas of a polished thin section used for microprobe analysis. The FIB device used was a FEI FIB200TEM. Details of the FIB milling are given in Wirth (2004, 2009). TEM investigations were performed in a FEI TECNAI F20 X-Twin transmission electron microscope with a field emission gun as electron source. Acceleration voltage was 200 kV. The instrument is equipped with a Gatan imaging filter (GIF, Tridiem), an EDAX X-ray analyzer with ultra-thin window and a Fishione high-angle annular dark field detector HAADF (Model 3000). Bright field and dark field images usually were acquired as energy filtered images applying a 20 eV window to the zero loss peak. Analytical electron microscopy (AEM) was

TABLE 2a. System without F: Run data, starting materials, and run products

Run no.	Time (days)	Rutile (mg)	Wollastonite (mg)	Al ₂ O ₃ (mg)	NaCl (mg)	H ₂ O (mg)	Product phases		
							Inner capsule + rutile+titanite	Outer capsule	Al in ttn (pfu)
Ttn4	1	29.8	37.48	12.89	43.22	45.31	prv	grs, cm, wo, cc	0.12–0.21
Ttn9	3	26.16	34.33	12.62	39.7	40.06	prv, cm	grs, an, cm, wo	0.08–0.12
Ttn8	7	26.82	34.33	12.33	46.33	51.51	prv, cm(q)	grs, an, wo, cm	0.12–0.23
Ttn1*	14	20.2	33.33	14.53	34.09	40.61	prv, cm(q)	grs, an, wo, cm, cc	0.11–0.21
RT22	30	46.17	64.04	38.52		122.37†	cm(q), cc	grs, an, wo (new and old), cc	0.09–0.11
RT16	60	59.14	59.88	30.48		136.94†	grs, cm(q)	grs, cm(q)	0.13–0.24
RT19	107	49.71	55.22	40.0		118.92†	cm(q)	grs, an, cm(q)	0.05–0.15

TABLE 2b. System with F: Run data, starting materials, and run products

Run no.	Time (days)	Rutile (mg)	Wollastonite (mg)	Al ₂ O ₃ (mg)	CaF ₂ (mg)	NaCl (mg)	H ₂ O (mg)	Product phases		
								Inner capsule + rutile+titanite	Outer capsule	Al in ttn (pfu)
Ttn7	1	19.13	35.82	9.0	3.85	36.0	21.56	prv, cm, fl	grs, an, ab, wo, fl, cm, cc, Al ₂ SiO ₅	0.35–0.47
Ttn10	3	20.71	34.27	12.31	5.55	40.61	43.55	prv, fl, cm	grs, an, wo, cm, fl	0.26–0.41
Ttn2	7	24.14	37.38	12.25	6.82	40.19	41.57	prv, cm, cc	an, ab, grs wo, cm, fl	0.24–0.38
Ttn12	14	17.6	30.36	11.74	8.1	34.31	37.54	prv, cm, fl	grs, an, fl, cm	0.26–0.48
RT23*	30	49.03	81.08	26.0	11.59		115.88†	cm(q)	grs, an, wo (new and old)	0.29–0.46
RT17	60	41.21	55.26	20.94	9.61		146.73†		grs, an, ab, cm	0.27–0.51
RT20*	107	53.3	52.40	32.87	12.8		113.34†	cm(q)	grs, an, fl	0.16–0.54

Notes: Abbreviations: ab = albite; an = anorthite (always close to end-member an >90), cc = calcite, cm = corundum, fl = fluorite, grs = grossular (in runs with fluorite: F-grossular), prv = perovskite, wo = wollastonite, (q) = quench. All experiments were carried out at 0.4 GPa and 600 °C. Variation of Al content in titanite is given for minimum and maximum values in cations per formula unit (pfu) (see Table 3); phases in the inner and outer capsule summarized from SEM and EMP.

* Partial weight loss after run.

† Total weight of H₂O+NaCl: H₂O was weighed in first and the same weight of NaCl added.

performed in the scanning transmission mode thus minimizing mass loss during spectrum acquisition (60–100 s). Natural starting materials were controlled with powder X-ray diffraction (XRD).

RESULTS

Run products in the inner (Pt) capsule

Run duration, initial composition, and run products in the inner and outer capsule are listed in Table 2; examples of the run products are shown in Figure 2. Experiments with and without CaF₂ resulted both in similar time-dependent overgrowth patterns on rutile. Complete overgrowth was not observed. Free rutile surfaces in contact with the fluid were present in all runs. They show rounded edges of terraced crystal surfaces typical of dissolution (Fig. 2i). Phases and their distribution on the surface of the rutile and in the run products outside the Pt capsule were controlled by SEM element mapping (Figs. 2a, 2b, and 2d; documentation of all runs in Appendix Fig. 1¹). Growth of titanite, and in short-time runs perovskite, occurs exclusively in the Pt capsule on the rutile surface, i.e., restricted to the site of the Ti source. Crystallographic orientation of the titanite is random as seen in the SEM images (Fig. 2). Preferred nucleation of titanite appears to be absent, and titanite grew similarly on broken surfaces and euhedral crystal faces. Titanite grain size increases up to >>100 μm and the number of crystals is reduced with longer run times (14, 30, 60, and 107 days). Perovskite on the rutile surface (Figs. 2a, 2b, and 2d) occurs in experiments with run times of up to 7 days, reacts into titanite in 14 days (Figs. 3d, 3e, and 3f), and is absent after 30 days (Fig. 4). The occurrence of abundant idiomorphic corundum and fluorite crystals (Fig. 2c)

on the rutile surface is also restricted to short run times (Table 2), but corundum is present as quench phase after longer run times (Fig. 2f). Occasional calcite grains are interpreted as impurities, possibly from the starting material wollastonite. A single grossular crystal (~50 μm) in the titanite overgrowth of run RT16 is a unique occurrence so far (Fig. 2g). All minerals on the surface appear as solitary idiomorphic crystals, in monomineralic groups, or in contact with each other.

In polished grain mounts, the thickness of the titanite overgrowths generally increases with run time (Figs. 3–4). Quantification, i.e., extrapolation from two to three dimensions, is hampered by the irregular shape of the incomplete overgrowth. Titanite grew also along fractures within some rutile grains and can result in extensive fragmentation of the rutile grain (Fig. 3d). Once commenced, fragmentation is a self-accelerating process due to the large differences between the molar volume of rutile (~18.8 cm³/mol; WWW-MINCRYST, RUTILE-4028) and titanite (~55.7 cm³/mol; WWW-MINCRYST, TITANITE-4764). The relations among titanite, perovskite, and rutile are best seen in element maps (Fig. 3). Perovskite and titanite in 7-day runs show straight grain boundaries indicating textural equilibrium, but perovskite is consumed to variable degree by titanite in the 14-day run (Fig. 3). Reactions are incomplete: some perovskite and titanite grains contain relicts of rutile. After 30, 60, and 107 days run time, only titanite was detected in the element distribution maps (Fig. 4). The very small and rare spots in the element maps with high F or Al (Fig. 4f) could indicate relicts of corundum or fluorite that are also rarely present at the surface in some long-time runs.

In titanite, the amount of Na and Cl (both present in the fluid) and Fe (present in the starting material rutile with up to 1 wt% FeO) are all below detection limit of the used EMP setup (Table 3). Iron is most likely sequestered into grossular and the Pt capsule. Al-free titanite did not form (Fig. 5), and titanite is always strongly zoned with respect to Al-Ti-F (Figs. 3–4). In

¹ Deposit item AM-10-051, Appendix Figures 1 and 2. Deposit items are available two ways: For a paper copy contact the Business Office of the Mineralogical Society of America (see inside front cover of recent issue) for price information. For an electronic copy visit the MSA web site at <http://www.minsocam.org>, go to the *American Mineralogist* Contents, find the table of contents for the specific volume/issue wanted, and then click on the deposit link there.

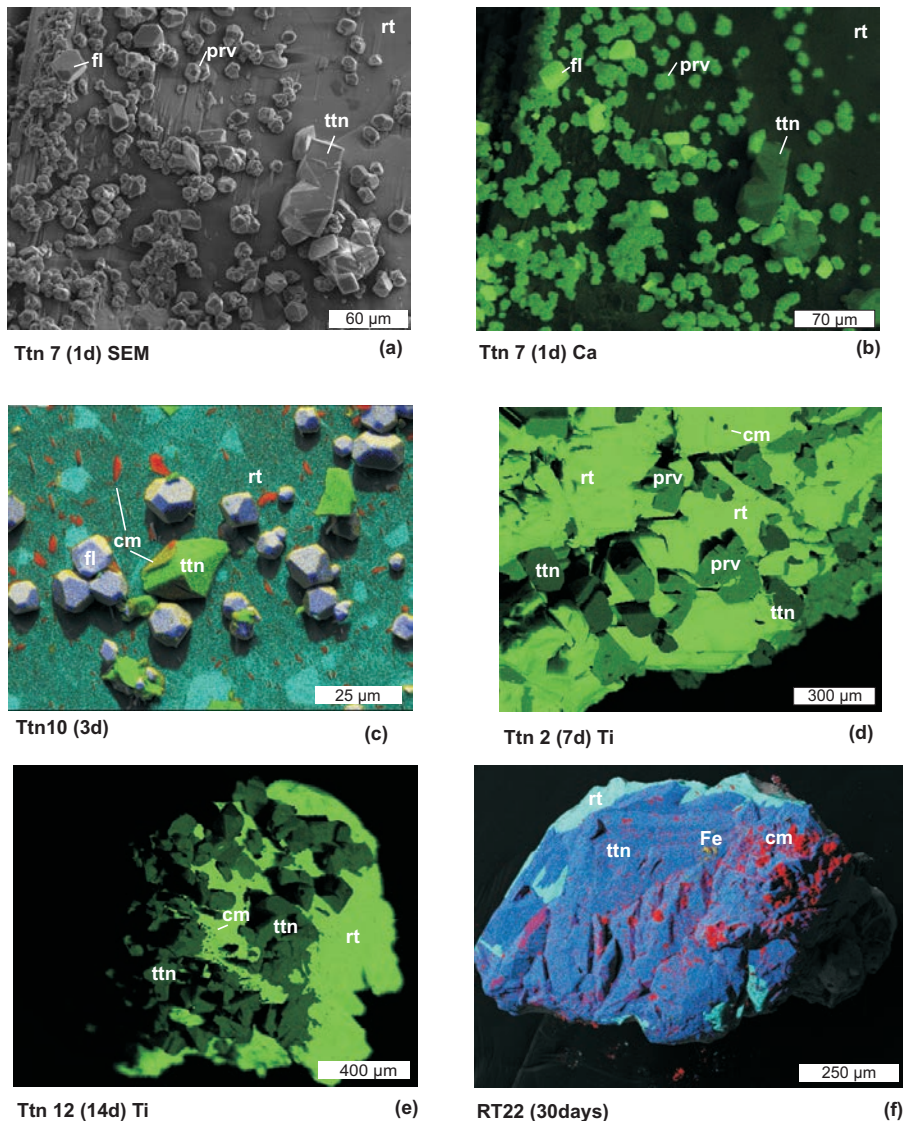


FIGURE 2. SEM images and SEM element distribution maps of run products on the rutile surface in the two systems (with and without F); note the different scales of the images. SEM image (a) and Ca distribution (b) from run Ttn7 (1 day), which distinguished between rutile (rt), titanite (ttn), perovskite (prv), fluorite (fl), and minor corundum (cm). (c) Run Ttn 10 (3 days) fluorite, titanite, and some corundum formed; clear turquoise patches on the rutile surface indicate former contacts between adhered minerals and rutile, accidentally removed during sample handling; the cloudy turquoise color of the free rutile surface is caused by fine-grained quench products. (d) Run Ttn2 (7 days); rutile, titanite, and perovskite are distinguished by their Ti contents. (e) Run Ttn12 (14 days); titanite is the dominant new Ti-phase on the rutile surface, but perovskite is still present within the titanite (see polished section Figs. 3d–3f). (f) Run RT22 (30 days); titanite covers large part of the rutile grain, but free rutile surfaces are still present. The abundant corundum and the Fe-rich stains are quench precipitates. (Continued on next page.)

runs with F, the maximum Al content is 0.5 Al pfu (Figs. 5a–5b) due to the preferred substitution $\text{Al}+\text{F} = \text{Ti}+\text{O}$. Without F, the maximum substitution $\text{Al}+(\text{OH}) = \text{Ti}+\text{O}$ is near 0.25 Al pfu (Fig. 5c). There is no systematic relation between run time and extent of the Al substitution. There is a large variation already after short run times, and after 107 days the whole range of compositions between 0.15 and 0.5 Al pfu is covered (Fig. 5). The analysis points plot near to the ideal substitution, but for the short-time runs they lie consistently above the ideal substitution line (Figs.

5b–5c), indicating a slight deviation from stoichiometry, which disappears with longer run time. The compositional zoning is not affected by this small change.

Element mapping (Figs. 3–4) shows the irregular distribution of Al, always inversely related to Ti and positively correlated with F. Areas with high-Ti (low-Al) content as well as with low Ti (high Al) occur next to rutile. Zones with high and low Ti concentration have sharp borders outlining lozenge-shaped areas, the typical cross-section of euhedral titanite, but appear also dif-

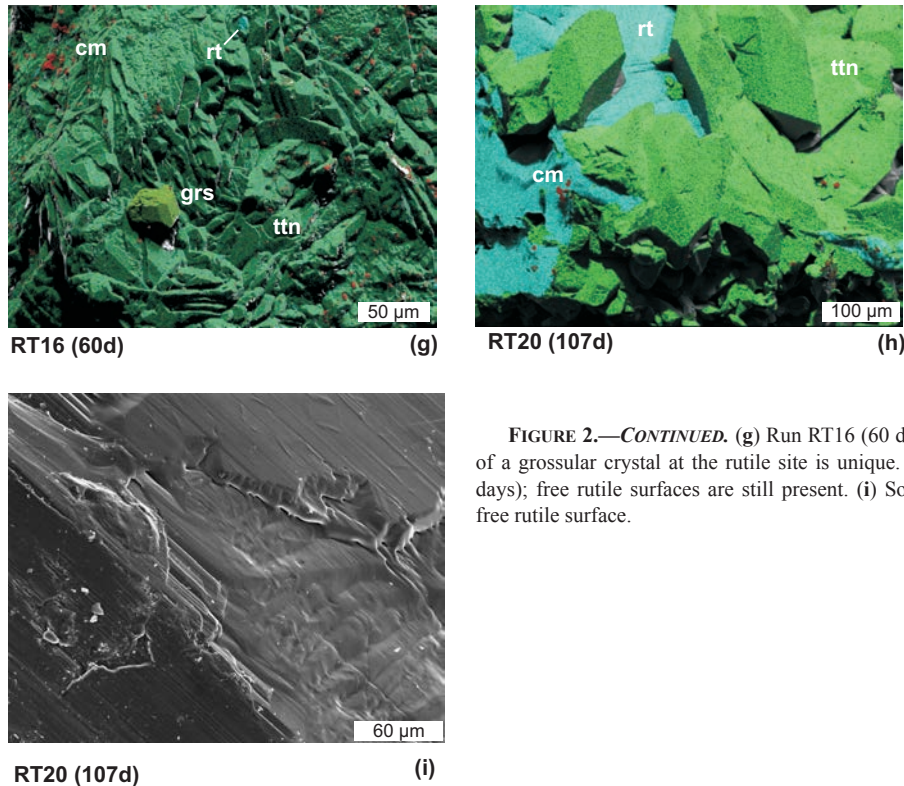


FIGURE 2.—*CONTINUED.* (g) Run RT16 (60 days); the occurrence of a grossular crystal at the rutile site is unique. (h) Run RT20 (107 days); free rutile surfaces are still present. (i) Solution features on a free rutile surface.

fuse. Around relict perovskite, which is replaced by titanite, there is also no systematic relationship of the Al-Ti content in titanite (Fig. 3). The Ti-distribution can be relatively homogeneous, but also patchy with both low- and high-Al areas next to perovskite. Run products from runs without F show the same irregular zoning of the Al content (Fig. 4e). Perovskite is nearly pure CaTiO_3 with minor Na (0.01–0.02 pfu; Table 4).

Run products in the outer (Au) capsule

Run products of wollastonite + $\gamma\text{-Al}_2\text{O}_3$ + fluid are grossular and anorthite (Fig. 6a–d; documentation of all runs in Appendix Fig. 1¹) of near end-member composition (Tables 5–6). Aluminum silicate was detected in run Ttn7 (1 day) by SEM. The $\gamma\text{-Al}_2\text{O}_3$ powder transformed into corundum, which remained present together with wollastonite in all short-time experiments (Figs. 6a–6d). In runs RT22 and 23, new wollastonite precipitated in the vicinity of the starting wollastonite. The addition of CaF_2 did not influence the formation of grossular and plagioclase. CaF_2 powder dissolved and formed idiomorphic fluorite crystals on the rutile surface and in the outer capsule already after short run time. Observations of polished grain mounts under the microscope and EMP and run products by SEM indicate rapidly decreasing contents of the starting materials corundum, wollastonite, and CaF_2 . In the long-time runs, grossular and plagioclase form large idiomorphic single crystals or aggregates (Figs. 6e–6g).

Grossular has near end-member composition in the F-free system (Table 5a) and contains between ~4 and ~12 mol% Ca-F-garnet component in the system with F (Table 5b). No systematic zoning in F was detected. FeO contents are low and

TiO_2 contents even lower, independent of the presence of F. Fe- and Ti-bearing garnet end-members are below 0.8 mol%, in most samples <0.5 mol%. Feldspar (Table 6) is anorthite with near end-member composition (except in run Ttn2 with Na ~1.7 wt% or 0.15 pfu, all other runs <0.06 pfu). Rarely a phase with a composition similar to albite-rich plagioclase, but imperfect stoichiometry (Al+Si slightly below 4; Na+Ca slightly higher 1) occurs together with anorthite. It was detected by EMP in runs Ttn2 (7 days) and RT17 (60 days).

TEM investigations

Representative FIB foils from three runs have been prepared. They show in many cases a tight phase boundary between titanite and rutile, but also a phase boundary with an approximately 150 nm wide area. This area is filled with an amorphous phase with a titanite-like composition (Fig. 7; more examples are documented in Appendix Fig. 2¹). Another type of porosity has been observed within titanite (Fig. 7). In the near two-dimensional section of the FIB foil it appears as holes, partly filled with NaCl crystals. It must be left open if they are channels or isolated fluid inclusions with daughter crystals. Overall, the microstructure of both titanite and rutile does not show remarkable features.

DISCUSSION

In a fluid-mediated growth of a crystal, the availability of the required elements in the fluid controls the growth. In the case of titanite, these are Ca, Si, and Ti as the essential elements, and Al and F (see Fig. 1 for the different element sources). Iron is present in small amounts in the starting material rutile, but could

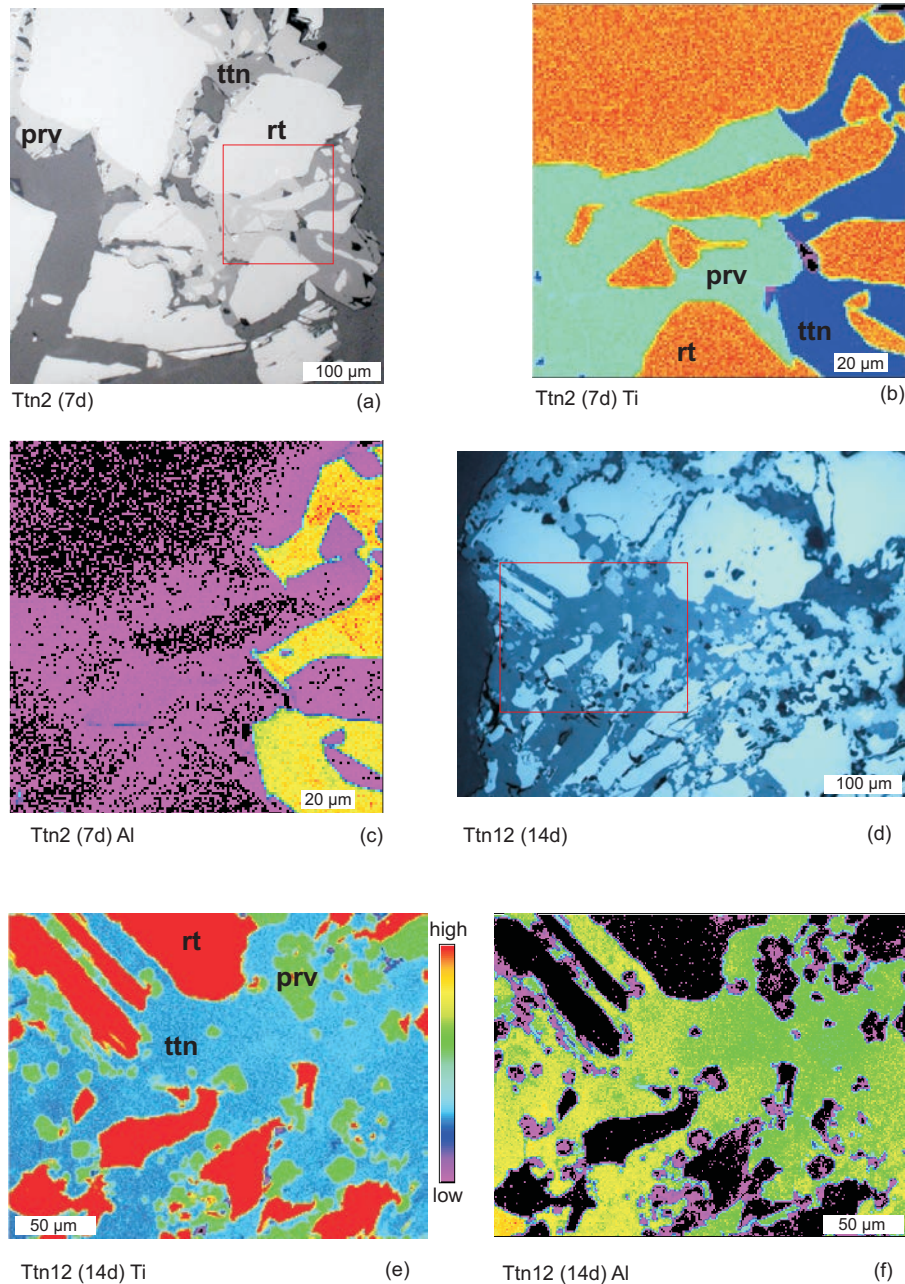


FIGURE 3. Photomicrographs (a, d) and EMP element distribution maps (b, c, e, f) of run Ttn2 (7days) and Ttn12 (14 days) from polished grain mounts. The insets in a and d mark the position of the EMP maps. (a) Run Ttn2; different grayscales distinguish rutile (rt; light gray), perovskite (prv; medium gray), and titanite (ttn; dark gray). Perovskite is the dominant new mineral. (b) Ti distribution: rutile, titanite, and perovskite are distinguished by their different Ti contents. (c) Al-distribution in titanite is irregular. (d) Run Ttn12; the rutile grain is fractured by the new-grown perovskite and titanite. (e, f) Ti distribution: perovskite is consumed by the abundant titanite. (f) Al-distribution in titanite is irregular and independent of the presence of relict perovskite.

not be found in significantly high amounts in the solids and is neglected in the further discussion. Sodium and Cl are important for complexing and thus for the solubility of the components (e.g., Newton and Manning 2006, 2007; Manning et al. 2008; Rapp et al. 2010), and although Na is present in small amounts in perovskite and anorthite, we assume that it is mainly present

in the fluid. Figure 8 shows schematically the situation at the site of the rutile crystal.

The solubility of Ca, Si, Al, and Ti differs strongly (see ref. above), and therefore their relative mobility is also different. In the F-free system, for 1 mole of titanite with 50 mol% Al-end-member $\text{CaTi}_{0.5}\text{Al}_{0.5}\text{SiO}_{4.5}(\text{OH})_{0.5}$ 1 mol CaSiO_3 + 0.25 mol Al_2O_3 ,

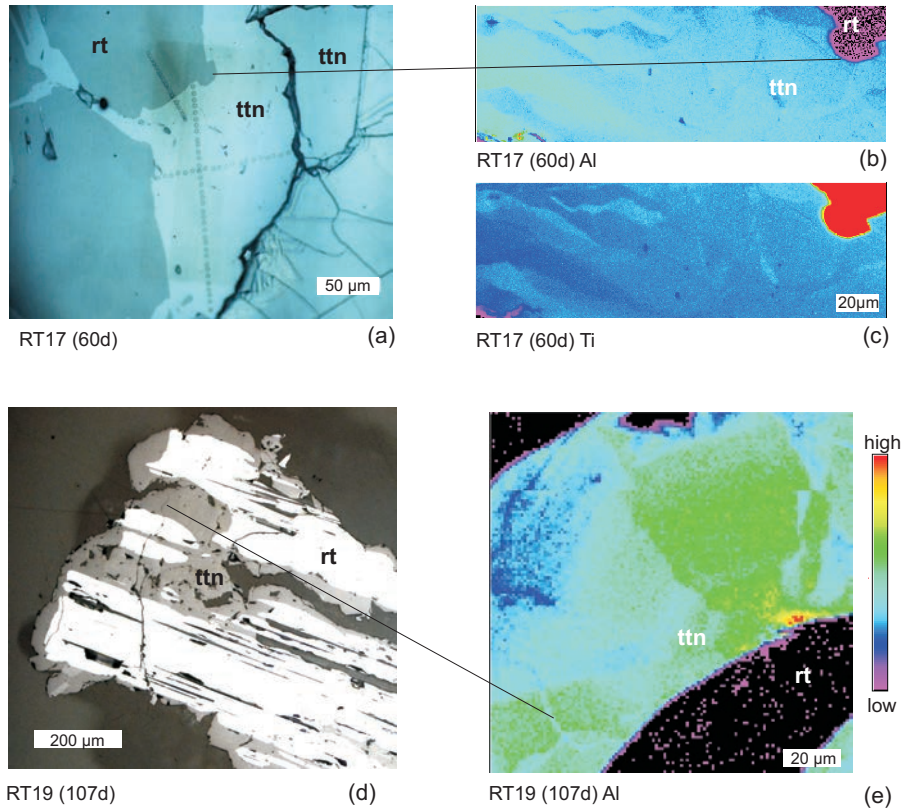


FIGURE 4. Photomicrographs (a, d) and EMP element mappings (b, c, e) of run products after 60 (RT17) and 107 (RT19) days run time; run RT17 with F, run RT19 without F. (a, d) Polished grain mounts, reflected light; the positions of the element maps are indicated by thin line; dots in a are marks of EMP analyses in the carbon coating. (b, e) Al distribution; (c) Ti distribution. The pattern of the zoning in titanite is irregular in both systems (with and without F).

TABLE 3a. Representative electron microprobe analyses of titanite for runs without F (mean errors of single analysis at given EMP setup and element concentrations: SiO₂ ~0.4%; TiO₂ ~0.5%; Al₂O₃ ~0.8% – ~1.5%; CaO ~0.6%)

Run no.	Ttn4		Ttn9		Ttn8		Ttn1		RT22		RT16		RT19	
Run duration	1		3		7		14		30		60		107	
Analysis no.	130	114	353	439	336	333	15	56	342	315	62	71	1	89
SiO ₂	29.87	29.59	30.14	29.77	30.24	30.53	29.96	30.41	30.44	29.73	30.53	30.35	31.01	31.03
TiO ₂	34.71	37.34	37.78	37.32	37.70	32.83	37.15	34.16	38.45	37.84	35.67	33.15	38.42	36.17
Al ₂ O ₃	5.23	3.54	2.74	3.31	3.15	6.67	3.79	5.54	2.55	2.95	3.47	6.19	1.67	3.86
CaO	28.88	28.99	29.13	28.37	29.36	29.34	29.50	30.09	29.56	29.47	28.44	28.30	29.01	28.82
Σ	98.69	99.46	99.79	98.77	100.45	99.36	100.40	100.20	101.00	99.99	98.11	97.99	100.11	99.88
Si	0.963	0.955	0.972	0.969	0.967	0.969	0.956	0.962	0.971	0.956	0.996	0.980	1.000	0.993
Ti	0.841	0.906	0.916	0.913	0.907	0.784	0.892	0.812	0.922	0.915	0.875	0.805	0.932	0.870
Al	0.199	0.135	0.104	0.127	0.119	0.250	0.143	0.206	0.096	0.112	0.133	0.236	0.063	0.146
Ca	0.997	1.002	1.006	0.989	1.006	0.998	1.009	1.019	1.010	1.015	0.994	0.979	1.003	0.988
OH calc	0.199	0.135	0.104	0.129	0.119	0.250	0.135	0.206	0.096	0.104	0.134	0.236	0.063	0.146

Note: Formula calculation based on Σ (cations) = 3.0; (OH) calculated.

+ 1 mol TiO₂ + 0.5 mol H₂O are required. Titanium is the least mobile component, because the formation of new Ti-minerals is restricted to the Ti-source on the rutile surface, and individual titanite and perovskite crystals were found neither in the inner nor in the outer capsule. Small Ti contents near the detection limit in grossular (Table 3) are the only indication for a small transport of Ti into the outer capsule. In contrast, the ED X-ray spectrum of grossular found within the titanite overgrowth (run RT16) shows a significant Ti peak (Appendix Fig. 1¹). Low Ti-mobility is consistent with available data about rutile solubility

(Ayers and Watson 1993; Audéat and Keppler 2005; Tropper and Manning 2005; Antignano and Manning 2008; Manning et al. 2008). Although the mentioned experimental studies differ in absolute amounts (as well as in applied *P-T-X*-conditions), they agree in the overall statement that solubility is low. Manning et al. (2008) made the important observation that in the Na-Al-bearing system albite-rutile the solubility of rutile is lower than in the Al-free Na-silicate-bearing system, but in the presence of Cl or F, solubility is strongly enhanced (Rapp et al. 2010).

Aluminum, which was often considered as rather immobile

TABLE 3b. Representative electron microprobe analyses of titanite for runs with F (mean errors of single analysis at given EMP setup and element concentrations: SiO₂ ~0.4%; TiO₂ ~0.5%; Al₂O₃ ~0.6% – ~1.0%; CaO ~0.6%; F ~1.5%)

Run no.	Ttn7		Ttn10		Ttn2		Ttn12		RT23		RT17/2		RT20	
Run duration	1		3		7		14		30		60		107	
Analysis no.	228	230	185	192	50	Pro7	Pro7	59	L2	L1	Pro7	Pro2	244	326
SiO ₂	30.70	31.52	31.32	31.57	30.81	31.39	31.39	32.11	30.37	30.67	31.39	31.84	31.08	32.28
TiO ₂	27.88	24.93	29.89	25.49	32.72	29.58	29.58	22.19	30.00	25.91	29.58	21.44	34.46	22.62
Al ₂ O ₃	9.31	11.15	7.71	11.07	6.85	7.69	7.69	13.05	7.79	11.33	7.69	13.60	4.35	13.16
CaO	28.75	29.43	29.24	29.32	28.34	28.98	28.98	29.44	28.76	29.83	28.98	29.44	29.09	29.52
F	2.90	3.86	2.37	3.07	2.16	2.33	2.33	4.15	2.83	3.67	2.33	4.67	1.13	4.38
Σ*	98.32	99.26	99.58	99.22	100.02	99.01	99.01	99.21	99.88	101.45	99.01	99.01	99.69	100.18
Si	0.986	0.996	0.997	0.995	0.984	1.004	1.004	1.006	0.979	0.963	1.004	1.000	0.998	1.003
Ti	0.673	0.592	0.715	0.604	0.786	0.712	0.712	0.523	0.727	0.612	0.712	0.506	0.833	0.529
Al	0.352	0.415	0.289	0.411	0.258	0.290	0.290	0.482	0.296	0.420	0.290	0.503	0.165	0.482
Ca	0.989	0.996	0.997	0.990	0.970	0.993	0.993	0.988	0.993	1.004	0.993	0.990	1.001	0.983
F	0.295	0.385	0.239	0.306	0.218	0.236	0.236	0.411	0.288	0.364	0.236	0.464	0.115	0.431
OH calc	0.058	0.030	0.051	0.105	0.041	0.055	0.055	0.071	0.011	0.056	0.055	0.040	0.050	0.052

Note: Formula calculation based on Σ(cations) = 3.0; (OH) calculated.

* Corrected for F.

TABLE 4. Representative electron microprobe analyses of perovskite (mean errors of single analysis at given EMP setup and element concentrations: Na₂O ~5.0% – ~8.0%; TiO₂ ~0.4%; CaO ~0.5%)

Run no.	Ttn4		Ttn7		Ttn9		Ttn10		Ttn2		Ttn1		Ttn12	
Run duration	1		1		3		3		7		14		14	
No F/with F	no F		with F		no F		with F		with F		no F		with F	
Number of analyses	9	1σ	1	1	19	1σ	13	1σ	56	1σ	7	1σ	31	1σ
Na ₂ O	0.226	0.030	0.256	0.223	0.044	0.225	0.056	0.301	0.071	0.100	0.047	0.233	0.047	
CaO	40.782	0.978	38.864	40.823	0.382	40.207	0.581	39.972	0.681	41.546	0.872	40.060	1.080	
TiO ₂	56.933	1.423	56.729	58.121	0.811	58.755	0.533	59.142	0.754	58.161	0.583	59.260	1.043	
Σ	99.542	1.953	96.256	99.751	0.770	99.295	0.954	99.438	0.576	101.107	0.344	99.553	0.580	
Na	0.010	0.001	0.012	0.010	0.002	0.010	0.002	0.013	0.003	0.004	0.002	0.010	0.002	
Ca	0.985	0.017	0.977	0.986	0.011	0.980	0.007	0.973	0.017	0.990	0.021	0.972	0.029	
Ti	0.966	0.017	1.001	0.986	0.011	1.005	0.003	1.010	0.009	0.973	0.010	1.009	0.014	
Σ cations	2.000	0.017	1.999	1.996	0.008	1.998	0.003	1.996	0.009	1.999	0.014	1.994	0.014	

Note: Formula calculation based on 3 oxygen atoms.

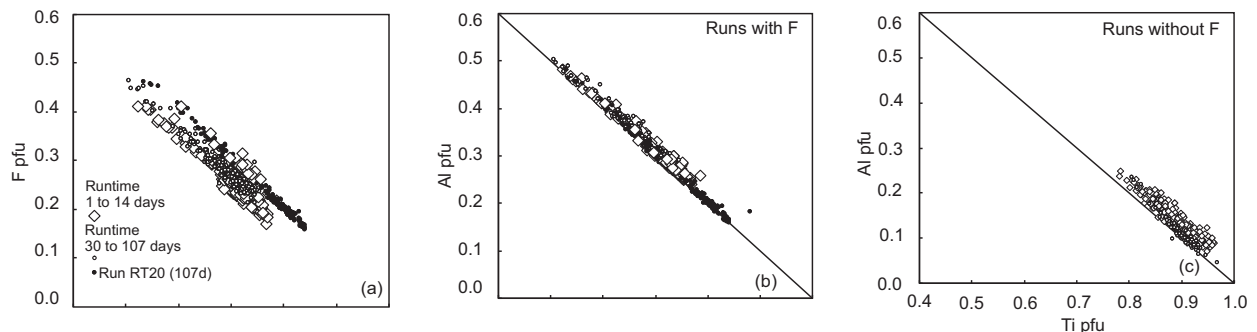
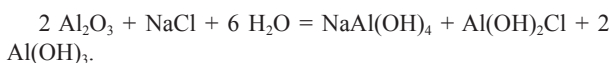


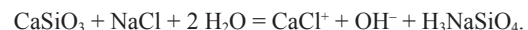
FIGURE 5. (a–c) Major element variability in titanite; short-time runs (1 to 14 days) and long-time runs (30 to 107 days) are distinguished. (a, b) Runs including fluorine (F) in the composition; run RT20 (107 days) is shown by black dots. (a) Variation of Ti and F; (b) of Ti and Al. (c) The substitution of Al for Ti is restricted in runs without F independent of the run time.

(e.g., Carmichael 1969), must be mobile in the experiments because, already after one day, high-Al titanite formed in the inner capsule and corundum formed as a transient phase on the rutile surface. High solubility of Al₂O₃ is also indicated by the presence of corundum as a quench phase in most runs (Table 2). Transport of Al probably occurs as NaAl(OH)₄ (Anderson and Burnham 1967; Walther 2001), and the actual dissolution reaction for Al₂O₃ according to Newton and Manning (2006) might be

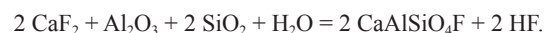


The source for Ca and Si is dissolution of wollastonite and its congruent dissolution in a NaCl-brine was described in Newton

and Manning (2006) and Fockenberg et al. (2006) as

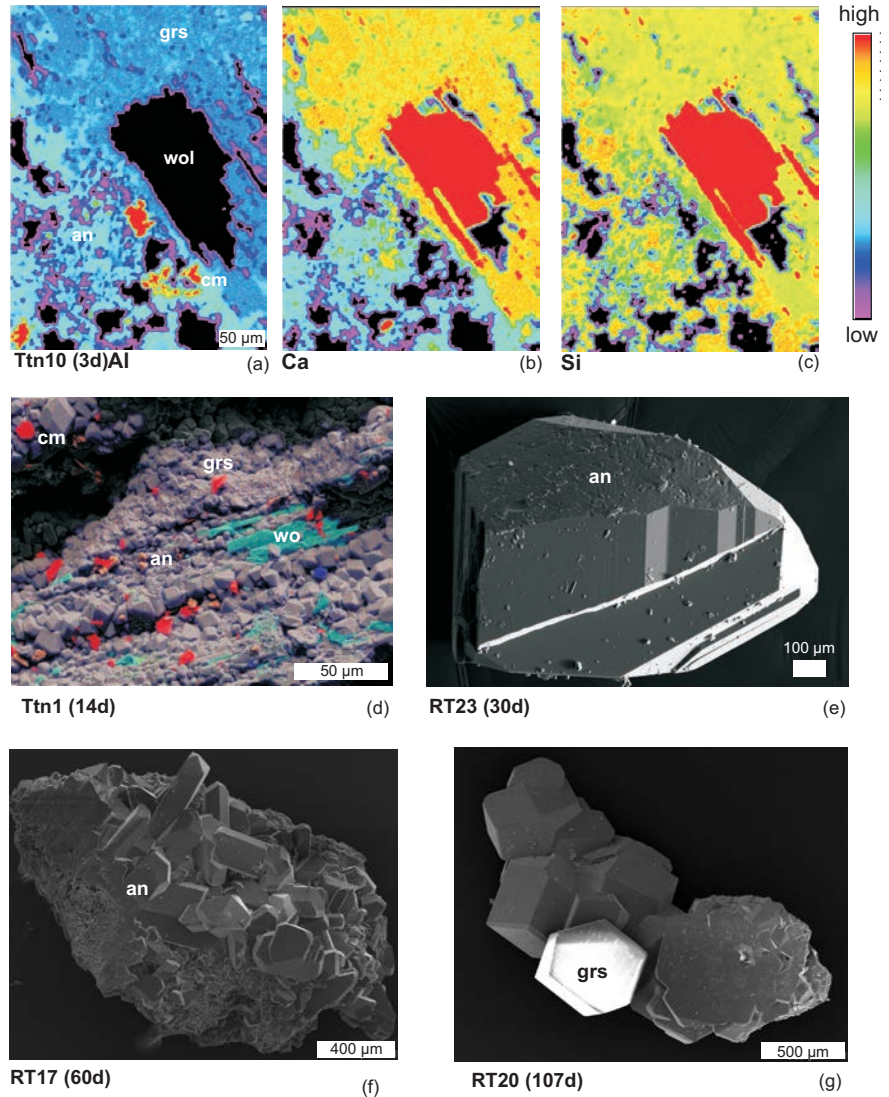


In the F-bearing system, the dissolution of fluorite is also a source for Ca for the 50 mol% Al-F-titanite. Fluorine was added as CaF₂ to allow for the formation of Al-F-titanite according to the end-member reaction



This reaction implies the formation of HF, which is assumed to be a highly mobile component in the hydrous fluid. Possibly fluorite is dissolved as CaClF+NaF in a NaCl-bearing

► **FIGURE 6.** (a–g) EMP element distribution maps (a–c), and SEM images (e–g), and SEM element distribution map (d) of run products of the outer capsule. Please mind the variable scale of the images. (a–c) Run Ttn10 (3days); Al (a), Ca (b), and Si (c) distribution distinguishes between wollastonite (wol) and Al₂O₃ (corundum; cm) and run products anorthite (an) and grossular (grs). (d) Run Ttn10 (3days) shows the distribution of phases on the surface of the run product. (e) Run RT23 (30 days), large solitary anorthite; (f) run RT17 (60 days), anorthite aggregate; (g) run RT20 (107 days), grossular aggregate.



fluid (Tropper and Manning 2007). These reactions will be representative for the first stages of the reaction, where wollastonite and Al₂O₃ (and CaF₂) are present, and provided that the congruent dissolution reactions are valid for the *P-T-X*-conditions of our experiments.

Metastable γ -Al₂O₃, used as starting material instead of the stable phase corundum α -Al₂O₃ to ensure a high solubility, was transformed already in the 1-day experiment into stable corundum. In the later stages of the experiment, most of the wollastonite and corundum reacted to grossular (\pm anorthite) in the outer capsule, and then the titanite-forming reaction is dominated by congruent dissolution of grossular (Fockenberg et al. 2008). Newton and Manning (2007) give a possible congruent dissolution reaction for grossular as one of several possibilities to formulate such a reaction at their run conditions of 800 °C/1 GPa:

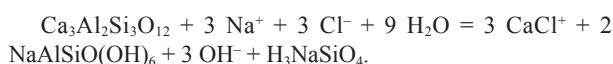


TABLE 5a. Grossular analyses: Representative electron microprobe analyses of grossular for runs without F (mean errors of single analysis at given EMP setup and element concentrations: SiO₂ ~0.4%; TiO₂ ~25%; Al₂O₃ ~0.5% – ~1.0%; FeO_{tot} ~15%; CaO ~0.5%)

Run no.	Ttn4	Ttn9	Ttn8	Ttn1	RT22	RT16	RT19
Run duration	1	3	7	14	30	60	107
SiO ₂	39.44	39.13	39.31	39.60	38.94	39.66	40.21
TiO ₂	0.01	b.d.	0.07	0.05	0.01	0.02	0.03
Al ₂ O ₃	22.52	23.42	23.01	23.17	23.10	22.33	22.65
FeO _{tot}	b.d.	0.17	b.d.	0.11	0.17	0.15	0.18
CaO	37.24	37.46	37.51	37.18	37.87	37.37	37.63
Σ	99.27	100.18	99.90	100.11	100.08	99.53	100.69
Si	2.977	2.926	2.948	2.965	2.914	2.989	2.995
Ti	0.001		0.004	0.003		0.001	0.001
Al	2.003	2.063	2.034	2.044	2.038	1.983	1.988
Fe ³⁺ _{calc}		0.011		0.007	0.011	0.010	0.011
Ca	3.011	3.000	3.014	2.982	3.037	3.018	3.004
End-members mol%							
Schorlomite-Al		0.4	0.2	0.1		0.1	0.1
Grossular	99.0	98.2	98.2	98.8	97.1	98.6	99.2
Andradite						0.5	0.6
Remainder	1.0	1.4	1.6	1.1	2.9	0.9	0.2

Notes: Formula calculation based on 8 cations and 12 oxygen; Fe³⁺ and end-member calculation according to Locock (2008); b.d. = below detection.

TABLE 5b. Grossular analyses: Representative electron microprobe analyses of grossular for runs with F (mean errors of single analysis see above)

Run no.	Ttn7	Ttn10	Ttn12	RT23	RT17	RT20
Run duration	1	3	14	30	60	107
Analysis no.	222	2	94	264	17	38
SiO ₂	35.90	36.16	37.90	35.91	36.68	37.29
TiO ₂	0.09	0.07	0.02	0.15	0.04	b.d.
Al ₂ O ₃	23.07	23.73	22.96	23.70	22.54	23.07
FeO _{tot}	b.d.	0.16	0.04	0.11	0.23	0.01
CaO	37.22	37.94	37.89	36.90	37.61	38.16
F	3.90	5.65	2.16	4.50	2.92	2.88
Σ*	98.57	101.32	100.06	99.37	98.79	100.20
Si	2.704	2.643	2.825	2.681	2.766	2.771
Ti	0.005	0.004	0.001	0.009	0.002	
Al	2.048	2.044	2.017	2.085	2.003	2.021
Fe ²⁺		0.001		0.004		
Fe ³⁺ _{calc}		0.009	0.002	0.003	0.015	
Ca	3.004	2.972	3.027	2.952	3.039	3.039
F	0.232	0.327	0.127	0.266	0.174	0.169
End-members mol%						
Ca-F-garnet	7.7	10.9	4.2	8.9	5.8	5.6
Schorlomite-Al	0.3	0.2	0.1	0.4	0.1	
Almandine		0.1		0.1		
Grossular	90.1	88.0	94.2	89.1	91.4	92.4
Andradite					0.7	
Remainder	2.0	0.9	1.6	1.5	1.9	2.0

Notes: Formula calculation based on 8 cations and 12 oxygen atoms; Fe³⁺ and end-member calculation according to Locock (2008); b.d. = below detection.

* Corrected for F.

It is not predictable, how anorthite behaves during the experiment. It dissolves incongruently (Roselle and Baumgartner 1995) and Al-silicate + quartz should form, which was found in only one run. Because the systems investigated here are under-saturated with respect to Si the formation of these breakdown products is unlikely.

Newton and Manning (2006) observed that with increasing NaCl content in the fluid, wollastonite and corundum solubility increases (whereas quartz solubility decreases strongly). Our experiments were carried out at high NaCl concentration, where solubility of Al and CaSiO₃ is high. The transient formation of perovskite CaTiO₃ indicates that Ca is more abundant at the reaction site than Si in the short-time runs. Probably the transport of CaCl⁻ is faster than that of H₃NaSiO₄ or Si remains in the outer capsule for the formation of grossular and anorthite. The transport of Al, possibly as NaAl(OH)₄, Al(OH)₂Cl, and/or Al(OH)₃ (Newton and Manning 2006) must be fast, because corundum precipitates at the rutile surface and high-Al-titanite already forms in the first days of the experiment. In the long-time experiments, perovskite reacts with Si to form titanite, and

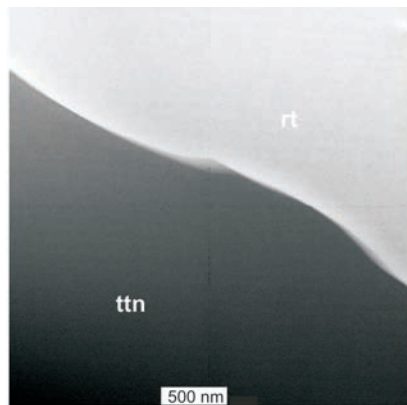
corundum to form more Al-titanite component. Therefore, during the experiments the relative sequence of mobility in the fluid is Ca ≈ Al ≈ Si > Ti. Further experiments have to be carried out, e.g., with grossular as the starting composition, to explore if reactions in the outer capsule (which simulates the rock matrix) are responsible for the occurrence of different phases in short- and long-time runs.

Irrespective of this question, the Al-Ti zoning in titanite, in short- and long-time runs, does not follow a systematic pattern, e.g., parallel to the euhedral outer faces of the growing titanite. It also does not follow the grain boundaries of the polycrystalline rim. A time-dependent Ti/Al evolution, e.g., a core-rim zoning of the large titanite in the long-time runs is absent. We use the term “patchy zoning” for this type of zoning. The *P* and *T* during growth of the crystals were maintained constant, and therefore the only remaining possibility to explain the variable Al-Ti content is a local control of the Ti and Al concentration. We propose a conceptual model for the growth of patchy zoning in titanite, assuming that Ti is the least soluble component and that the zoning is dominated by growth from the fluid, not dominated by diffusional processes. We take the exclusive occurrence of Ti-minerals on the surface of the rutile as evidence that the highest concentrations of Ti are restricted to the vicinity of the dissolving rutile (Fig. 8), i.e., dissolved Ti did not move far from the rutile. Although in the presence of Cl and F, the solubility of Ti is larger than without the complexing anions (Rapp et al. 2010), it is not transported away, whereas Al, Ca, Si, and F are rapidly transported to the reaction site at the rutile surface. At the rutile surface, the first titanite crystals grow rapidly from the fluid and the size of 100 μm is already reached after 1 day. Changes in the Ti/Al of the local fluid (in the vicinity of the rutile; Fig. 8) are recorded by the titanite composition. Changes in the Ca/Si of the fluid are recorded by the transitional mineral association including perovskite and fluorite, which precipitated on the rutile (Fig. 2; Appendix Fig. 1¹). The Ca/Si ratio of the fluid is high as long as reaction progress in the outer system for the formation of new minerals is fast, including recrystallization of the initial wollastonite. The consumption of perovskite in the 14 days runs by titanite requires a change in the fluid composition to lower Ca/Si ratios, which, however, does not influence the Ti-Al distribution in titanite. Considering the Al excess, the Ti/Al ratio is dominated by local variation of Ti-concentration available from rutile dissolution (Fig. 8). We speculate that the specific condition for titanite growth at the rutile site is the availability of Ca, Si, and Al (and F and OH for charge balance of the Al

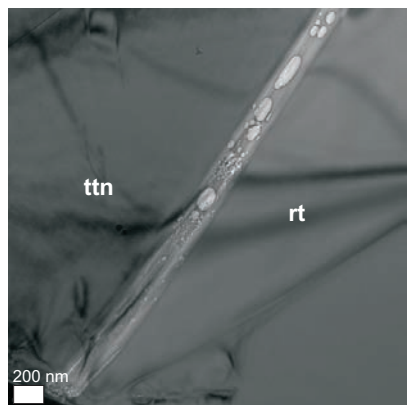
TABLE 6. Representative electron microprobe analyses of plagioclase from runs with and without F; formula calculation based on five cations (mean errors of single analysis see above)

Run no.	Ttn4	Ttn7	Ttn9	Ttn10	Ttn8	Ttn2	Ttn2*	Ttn12	RT22	RT23	RT17	RT17*	RT19	RT20
Run duration	1	3	3	7	7	14	30	30	60	60	107	107	107	107
with F/no F	no F	with F	no F	with F	no F	with F	with F	with F	no F	with F	with F	with F	no F	with F
Na ₂ O	0.17	1.23	0.55	0.53	0.65	1.73	8.38	0.62	0.57	0.22	0.22	11.20	0.17	0.20
CaO	20.08	19.27	19.29	19.61	19.13	17.65	5.89	42.82	19.51	19.81	19.89	2.31	20.08	20.00
Al ₂ O ₃	36.81	36.07	37.22	37.01	36.68	35.76	26.13	19.09	36.49	37.37	35.59	21.32	36.81	36.90
SiO ₂	43.41	44.18	43.39	43.47	43.73	45.12	60.41	36.62	42.27	42.93	43.69	67.67	43.41	43.89
Σ	100.45	100.76	100.46	100.71	100.20	100.26	100.80	99.16	98.85	100.34	99.39	102.50	100.45	100.99
Na	0.015	0.109	0.049	0.047	0.058	0.153	0.714	0.056	0.051	0.020	0.020	0.928	0.015	0.018
Ca	0.990	0.941	0.948	0.962	0.943	0.863	0.277	0.950	0.974	0.977	0.992	0.106	0.990	0.981
Al	1.997	1.938	2.012	1.998	1.988	1.924	1.354	2.005	2.005	2.027	1.954	1.074	1.997	1.992
Si	1.998	2.013	1.990	1.990	2.011	2.060	2.655	1.989	1.970	1.976	2.034	2.892	1.998	2.010

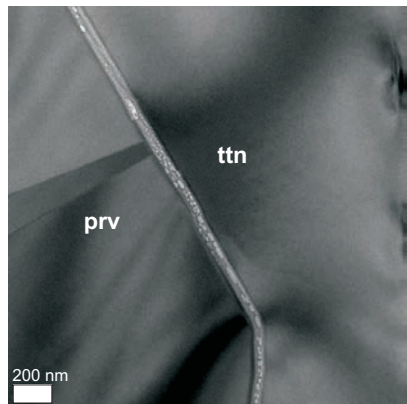
* Na-rich, feldspar-like composition.



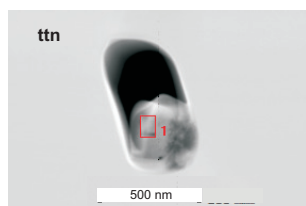
Ttn2 (7d) (a)



Ttn2 (7d) (b)



Ttn12 (14d) (c)



RT17 (60d) (d)

◀ **FIGURE 7.** TEM images of run products from runs Ttn2, Ttn12, and RT17. (a) Ttn2 (7 days) rutile (rt) and titanite interface: closed grain boundary (TEM foil 1931, prepared by FIB). (b) Ttn2 (7d) rutile (rt) and titanite interface: open grain boundary with amorphous phase and pores (TEM foil 1927). White ellipsoidal features are bubble-like thinner areas (pores) within an amorphous matrix. The diffraction contrast in both crystals ends abruptly at the crystal edge and is not continuing in the amorphous part thus indicating the amorphous state of the bubble-rich zone. The amorphous phase contains Si, Ca, and Ti, as determined by EDAX, in proportions that are approximately equivalent to mixtures of rutile and titanite. (c) Ttn12 (14 days) perovskite (prv) and titanite interface: open grain boundary with amorphous phase and pores (TEM foil 1932) similar to the observation in c. The chemical composition of the amorphous phase corresponds to a mixture of perovskite and titanite. (d) RT17 (60 days) HAADF image of a partly filled pore at a titanite-titanite grain boundary; (TEM foil 1937). The square marks the area sampled by an EDAX spectrum indicating a NaCl-crystal with some background of Ca-Si-Ti-Al.

incorporation), which are always provided via fluid (according to the high solubility of the respective source minerals) from the outer capsule representing the “whole rock system.” “Slow” Ti does not have the chance to move along a concentration gradient, but is consumed “in situ” if a favorable concentration is reached. The compositional variation of the titanite should be a direct measure of the local fluid heterogeneity on a millimeter to micrometer scale. It is impossible to quantify the underlying process because the solubility of the different components in the complex fluid is unknown at the high P - T conditions of 0.4 GPa and 600 °C.

Transport of Ti to the reaction site is easy because free rutile surfaces are always present in the experiments. The dissolution of rutile is easier at these free surfaces than on the relatively tight phase boundary with the growing titanite. However, some transport is also possible along the grain boundaries and porosities in titanite (Fig. 7). The reaction progress will only be dominated by these transport paths, when the relict rutile is completely covered by titanite. Cracking of the rutile crystals due to volume expansion during the reaction from rutile to titanite will create new free rutile surfaces, and it is assumed that the whole reaction proceeds rapidly, as long as a fluid phase is present. Considering the short run time of our experiments in comparison with geological processes, the reaction seems more or less instantaneous. We can conclude that in all cases where we see in rocks the reaction of rutile into titanite as a reaction rim, i.e., relict rutile is preserved, this reaction stopped because the fluid was either consumed or rutile as the Ti source effectively sealed. In the case of small rutile relics in titanite crystals, one can speculate that pathways through the titanite were insufficient for element transport.

CONCLUDING REMARKS

Zoning in metamorphic minerals is a powerful tool for reconstructing the P - T - X variables during mineral growth [for a review see Kohn (2003)]. Regular core-rim zoning has been explained by Rayleigh fractionation in combination with a continuous change of P - T conditions, absence of zoning in minerals such as garnet, which are commonly zoned, explained by diffusion processes at high (granulite-facies) temperature. Both processes can be

excluded for the results of our experiments because a strong, but irregular patchy Ti-Al-F-OH zoning formed in titanite without a change in the P - T conditions. Diffusion on a time scale of <107 days can safely be neglected at 600 °C as a major modifying process. In hydrothermal synthesis and crystal growth experiments, heterogeneous run products can be expected, when components with strongly different solubility are involved in fluid-mediated reactions (Zimmermann et al. 1996; von Goerne et al. 1999) except when starting from a homogeneous glass or gel. Different solubility and mobility of $\text{Ca} \approx \text{Al} \approx \text{Si} > \text{Ti}$ are responsible for the reaction progress. A fluid-mediated growth can produce patchy-irregular zoning, due to timely and locally varying Ti/Al in the vicinity of a dissolving rutile. This differs significantly from exchange reactions by dissolution and precipitation, which produce a core-rim zoning parallel to a sharp reaction front as a replacement process [for a summary see Putnis (2009)]. The titanite-forming process differs also completely from phase separation of a solid solution driven by a fluid interaction, as described for monazite-xenotime (Seydoux-Guillaume et al. 2007; Hetherington and Harlov 2008) or for apatite (Harlov et al. 2002, 2003, 2005). In the case of Al-titanite, the solid solution is formed during the growth of the crystal. The resulting zoning pattern might, however, be similarly irregular.

The patchy Al-Ti zoning patterns in the experimentally produced titanite and in natural titanite growing on rutile are strikingly similar (Fig. 9). The Ti source for the natural titanite overgrowth is localized in the rutile crystal, similar as in the experiments, whereas the Ca-Si-Al-OH-F supply depends on a

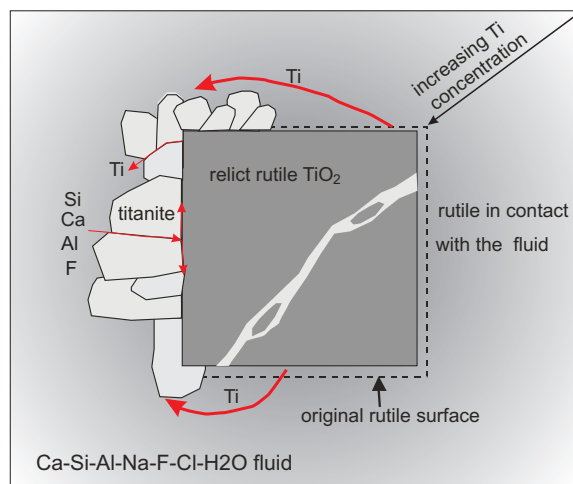


FIGURE 8. Sketch of the conditions for titanite formation from rutile during the experiment, for the F-free and for the F-bearing system. Formation of titanite occurs as an incomplete cover around the relict rutile, but also within stress-induced cracks in rutile, according to the volume change during the reaction of rutile into titanite. The reaction front is moving from the original rutile surface inside and outside. The polycrystalline titanite rim has euhedral outer shapes (compare Fig. 2). A free rutile surface is always preserved, enabling Ti dissolution and fast transport to the growing titanite crystals. Al, Si, and Ca also have to be transported through the rim toward the inner reaction front, Ti outward toward the growing titanite crystals.

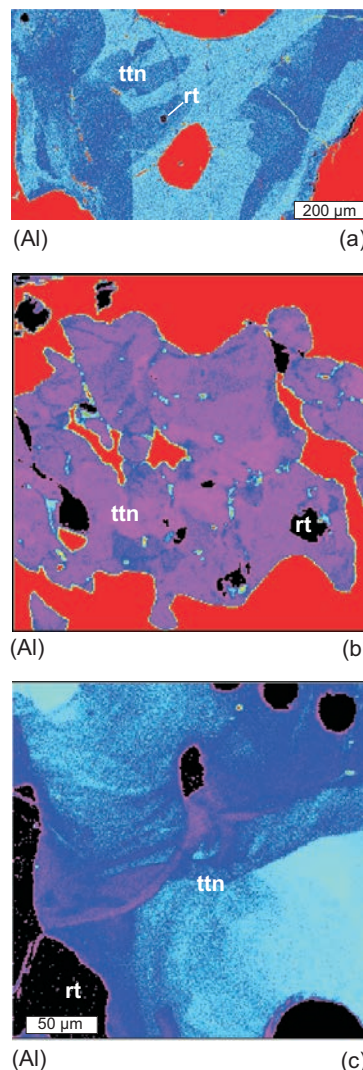


FIGURE 9. Element distribution maps showing patchy zoning of Al distribution in natural titanite overgrowth on rutile; compare Figure 4 for synthetic titanite. (a) Metabasite from Sierra Limon Verde, N Chile. Peak metamorphic conditions were $T \sim 660$ to 720 °C and $P \sim 1.3$ GPa (Lucassen et al. 1999). (b) Gneiss from Sierra Espinal, NW Argentina, metamorphic peak conditions $T > 650$ °C and $P \sim 0.5$ GPa (Lucassen and Becchio unpublished data). (c) Amphibolite-facies retrogressed eclogite from the Tromso area, Norway (e.g., Krogh et al. 1990).

fluid phase sampling a much larger rock volume. None of the Al distribution patterns in natural titanite is easily explained by solid-state diffusion along a gradient and we assume a growth pattern without major modification by solid-state diffusion. The element distribution pattern clearly excludes a Rayleigh fractionation process, commonly assumed to be responsible for the prograde zoning in garnet (Hollister 1966). Titanite with relicts of rutile indicate that the reaction stopped, most likely because the fluid was consumed, indicating a limited amount of fluid, invading a formerly dry rock volume during retrogression. Alternatively, fluid can be produced within a rock, e.g., during decompression from high pressure by breakdown of hydrous

phases such as phengite, producing small amounts of fluid in specific sites within the rock. It seems likely that such a fluid is heterogeneous in space and time. Heterogeneous fluids in rocks have been a matter of discussion in the literature. Selverstone et al. (1992) have argued for fluid heterogeneities at the scale of a thin section by analyzing the phase relations and reconstructing the composition of the fluid in equilibrium with the respective solid assemblage; here we can show experimentally that such fluid heterogeneities exist even on a much smaller scale.

Patchy zoning of Al-F-Ti in titanite has been explained as a combination of variation in P - T and fluid composition, especially in F (Franz and Spear 1985). However, as long as a fluid of appropriate composition is present, the reaction is very fast. The experiments show that already after one day reaction time a titanite crystal of $\sim 100 \mu\text{m}$ size can grow. This means that the variable composition of the patchy zoning in natural rock does not necessarily reflect variations of P and T , unless we assume a multi-stage scenario with an influx of a fluid into a rock, reaction until the fluid is consumed, then variation of P and T and an additional influx of fluid. Equilibration of Al-Ti zoning by solid-state diffusion after growth also appears to be of minor influence even on a geological time scale at amphibolite facies or lower T where most fluid-induced retrogression occurs.

The patchy zoning in natural and experimental samples appears to be linked to specific conditions of Ti immobility or mobility. Titanium is considered as relatively immobile in natural metamorphic environments in general (e.g., Van Baalen 1993). However, mobility of Ti from rutile dissolution has been occasionally observed in nature on various scales (thin section to meters) under favorable conditions, such as strong changes in P - T and related fluid flow (e.g., Gao et al. 2007; Luvizotto and Zack 2009). We speculate that this could be an effect of the composition of the Ti-mobilizing fluid phase (beside changing P - T conditions, that may limit the stability of titanite): low abundance of Ca could favor the mobilization of Ti, whereas a high abundance could favor precipitation of titanite at the site of the Ti source and immobilize Ti. Such an immobilization of Ti is common in metamorphic rocks during retrogression and observed, e.g., in titanite around high- T phases as Ti-rich biotite or hornblende.

ACKNOWLEDGMENTS

This work was carried out as part of the research group FOR 741 "Nanoscale processes and geomaterials properties," sponsored by DFG code number DFG grant DR 744/3-1. We thank our colleagues of FOR 741 for stimulating discussions and M. Gottschalk for the determination of the lattice constants of wollastonite. Careful reviews by P. Tropper and R.K. Popp are gratefully acknowledged. C. Zecha prepared the polished grain mounts, O. Appelt, J. Nissen, and F. Galbert provided their help with SEM and EMPA.

REFERENCES CITED

- Anderson, G.M. and Burnham, C.W. (1967) Reaction of quartz and corundum with aqueous chloride and hydroxide solutions at high temperatures and pressures. *American Journal of Science*, 265, 12–27.
- Antignano, A. and Manning, C.E. (2008) Rutile solubility in H_2O , H_2O - SiO_2 , and H_2O - $\text{NaAlSi}_3\text{O}_8$ fluids at 0.7–2.0 GPa and 700–1000 °C: Implications for mobility of nominally insoluble elements. *Chemical Geology*, 255, 283–293.
- Aranovich, L.Y. and Newton, R.C. (1996) H_2O activity in concentrated NaCl solutions at high pressures and temperatures measured by the brucite-periclase equilibrium. *Contributions to Mineralogy and Petrology*, 125, 200–12.
- Audétat, A. and Keppler, H. (2005) Solubility of rutile in subduction zone fluids, as determined by experiments in the hydrothermal diamond anvil cell. *Earth and Planetary Science Letters*, 232, 393–402.
- Ayers, J.C. and Watson, E.B. (1993) Rutile solubility and mobility in supercritical aqueous fluids. *Contributions to Mineralogy and Petrology*, 114, 321–330.
- Carmichael, D.M. (1969) On the mechanism of prograde metamorphic reactions in quartz-bearing pelitic rocks. *Contributions to Mineralogy and Petrology*, 88, 244–267.
- Castelli, D. and Rubatto, D. (2002) Stability of Al- and F-rich titanite in metacarbonate: petrologic and isotopic constraints from a polymetamorphic eclogite marble of the internal Sesia Zone (Western Alps). *Contributions to Mineralogy and Petrology*, 142, 627–639.
- Enami, M., Suzuki, K., Liou, J.G., and Bird, D.K. (1993) Al- Fe^{3+} and F-OH substitutions in titanite and constraints on their P-T dependence. *European Journal of Mineralogy*, 5, 219–231.
- Fockenber, T., Burchard, M., and Maresch W.V. (2006) Experimental determination of the solubility of natural wollastonite in pure water at pressures of 5 GPa and at temperatures of 400 to 800°C. *Geochimica et Cosmochimica Acta*, 70, 1796–1806.
- (2008) The solubility of natural grossular-rich garnet in pure water at high pressures and temperatures. *European Journal of Mineralogy*, 20, 845–855.
- Franz, G. and Spear, F.S. (1985) Aluminous titanite (sphene) from the Eclogite Zone, South-Central Tauern Window, Austria. *Chemical Geology*, 50, 33–46.
- Frost, B.R., Chamberlain, K.R., and Schumacher, J.C. (2000) Sphene (titanite): Phase relations and role as a geochronometer. *Chemical Geology*, 172, 131–148.
- Gao, J., John, T., Klemd, R., and Xiong, X. (2007) Mobilization of Ti–Nb–Ta during subduction: Evidence from rutile-bearing dehydration segregations and veins hosted in eclogite, Tianshan, NW China. *Geochimica et Cosmochimica Acta*, 70, 4974–4996.
- Hetherington, C.J. and Harlow, D.E. (2008) Metasomatic thorite and uraninite inclusions in xenotime and monazite from granitic pegmatites, Hydra anorthosite massif, southwestern Norway: Mechanics and fluid chemistry. *American Mineralogist*, 93, 806–820.
- Harlow, D.E., Förster, H.-J., and Nijland, T.G. (2002) Fluid-induced nucleation of (Y+REE) phosphate minerals in apatite. *Nature and experiment. Part I: Chlorapatite. American Mineralogist*, 87, 245–261.
- Harlow, D.E., Förster, H.-J., and Schmidt, C. (2003) High P-T experimental metasomatism of a fluorapatite with significant britholite and fluorellestadite components: implications for LREE mobility during granulite-facies metamorphism. *Mineralogical Magazine*, 67, 61–72.
- Harlow, D.E., Wirth, R., and Förster, H.-J. (2005) An experimental study of dissolution-precipitation in fluorapatite: Fluid infiltration and the formation of monazite. *Contributions to Mineralogy and Petrology*, 150, 268–286.
- Hollister, L.S. (1966) Garnet zoning: an interpretation based on the Rayleigh fractionation model. *Science*, 154, 1647–1651.
- Hunt, J.A. and Kerrick, D.M. (1977) The stability of sphene: experimental re-determination and geologic implications. *Geochimica et Cosmochimica Acta*, 41, 279–288.
- Kohn, M.J. (2003) Geochemical zoning in metamorphic minerals. In R. Rudnick, Ed., *Treatise on Geochemistry* 3, p. 229–261. Elsevier, Amsterdam.
- Krogh, E.J., Andresen, A., Bryhni, I., Broks, T.M., and Kristensen, S.E. (1990) Eclogites and polyphase P - T cycling in the Caledonian uppermost allochthon in Tromsø, northern Norway. *Journal of Metamorphic Geology*, 8, 289–309.
- Locock, A.J. (2008) An Excel spreadsheet to recast analyses of garnet into end-member components, and a synopsis of the crystal chemistry of natural silicate garnets. *Computers and Geosciences* 34, 1769–1780.
- Lucassen, F., Franz, G., and Laber, A. (1999) Permian high pressure rocks—The basement of Sierra de Limon Verde in N-Chile. *Journal of South American Earth Sciences*, 12, 183–199.
- Lucassen, F., Dulski, P., Abart, R., Franz, G., Rhede, D., and Romer R.L. (2010) Redistribution of HFSE elements during rutile replacement by titanite. *Contributions to Mineralogy and Petrology*, 160, 279–295, DOI: 10.1007/s00410-009-0477-3.
- Luvizotto G.L. and Zack, T. (2009) Nb and Zr behaviour in rutile during high-grade metamorphism and retrogression: An example from the Ivrea–Verbano Zone. *Chemical Geology*, 261, 303–317.
- Manning, C.E. and Bohlen, S.R. (1991) The reaction titanite + kyanite = anorthite + rutile and titanite-rutile barometry in eclogites. *Contributions to Mineralogy and Petrology*, 109, 1–9.
- Manning, C.E., Wilke, M., Schmidt, C., and Cauzid, J. (2008) Rutile solubility in albite- H_2O and $\text{Na}_2\text{Si}_2\text{O}_7$ - H_2O at high temperatures and pressures by in-situ synchrotron radiation micro-XRF. *Earth and Planetary Science Letters*, 272, 730–737.
- Markl, G. and Piazzolo, S. (1999) Stability of high-Al titanite from low pressure calcilcates in light of fluid and host-rock composition. *American Mineralogist*, 84, 37–47.
- Newton, R.C. and Manning, C.E. (2006) Solubilities of corundum, wollastonite and quartz in H_2O -NaCl solutions at 800 °C and 10 kbar: Interaction of simple minerals with brines at high pressure and temperature. *Geochimica Cosmochimica Acta*, 71, 5571–5582.
- (2007) Solubility of grossular, $\text{Ca}_3\text{Al}_2\text{Si}_2\text{O}_{12}$, in H_2O -NaCl solutions at 800

- °C and 10 kbar, and the stability of garnet in the system $\text{CaSiO}_3\text{-Al}_2\text{O}_3\text{-H}_2\text{O-NaCl}$. *Geochimica Cosmochimica Acta*, 70, 5191–5202.
- (2010) Role of saline fluids in deep-crustal and upper-mantle metasomatism: Insights from experimental studies. *Geofluids*, 9, 1–15.
- Oberti, R., Smith, D.C., Rossi, G., and Caucia, F. (1991) The crystal chemistry of high-aluminum titanites. *European Journal of Mineralogy*, 3, 777–792.
- Pouchou, J.L. and Pichoir, F. (1988) A simplified version of the ‘PAP’ model for matrix correction in EPMA. In D.E. Newbury, Ed., *Microbeam Analysis*, p. 315–318. San Francisco Press, California.
- Putnis, A. (2009) Mineral replacement reactions. In E.H. Oelkers and J. Schott, Eds., *Thermodynamics and Kinetics of Water-Rock Interaction*, 70, p. 87–124. *Reviews in Mineralogy and Geochemistry*, Mineralogical Society of America, Chantilly, Virginia.
- Rapp, J.F., Klemme, S., Butler, I.B., and Harley, S.L. (2010) Extremely high solubility of rutile in chloride and fluoride-bearing metamorphic fluids: An experimental investigation. *Geology*, 38, 323–326.
- Roselle, G.T. and Baumgartner, L.P. (1995) Experimental determination of anorthite solubility and calcium speciation in supercritical chloride solutions at 2 kb from 400 to 600 °C. *Geochimica et Cosmochimica Acta*, 59, 1539–1549.
- Seifert, W. and Kramer, W. (2003) Accessory titanite: An important carrier of zirconium in lamprophyres. *Lithos*, 71, 81–98.
- Selverstone, J., Franz, G., Thomas, S., and Getty, S. (1992) Fluid variability in 2 GPa eclogites as an indicator of fluid behavior during subduction. *Contributions to Mineralogy and Petrology*, 112, 341–357.
- Seydoux-Guillaume, A.-M., Wirth, R., and Ingrin, J. (2007) Contrasting response of ThSiO_4 and monazite to natural irradiation. *European Journal of Mineralogy*, 19, 7–14.
- Sourirajan, S. and Kennedy, G.C. (1962) The system $\text{NaCl-H}_2\text{O}$ at elevated temperatures and pressures. *American Journal of Science*, 260, 115–141.
- Troitzsch, U. and Ellis, D.J. (2002) Thermodynamic properties and stability of AlF-bearing titanite $\text{CaTiOSiO}_4\text{-CaAlFSiO}_4$. *Contributions to Mineralogy and Petrology*, 142, 543–563.
- Tropper, P. and Manning, C.E. (2005) Very low solubility of rutile in H_2O at high pressure and temperature, and its implications for Ti mobility in subduction zones. *American Mineralogist*, 90, 502–505.
- (2007) The solubility of fluorite in H_2O and $\text{H}_2\text{O-NaCl}$ at high pressure and temperature. *Chemical Geology*, 242, 299–306.
- Tropper, P., Manning, C., and Essene, E.J. (2002) The substitution of Al and F in Titanite at high pressure and temperature: experimental constraints on phase relations and solid solution properties. *Journal of Petrology*, 43, 1787–1814.
- Van Baalen, M.R. (1993) Titanium mobility in metamorphic systems: a review. *Chemical Geology*, 110, 233–249.
- von Goerne, G., Franz, G., and Wirth, R. (1999) Hydrothermal synthesis of large dravite crystals by the chamber method. *European Journal of Mineralogy*, 11, 1061–1078.
- Walther, J.V. (2001) Experimental determination and analysis of the solubility of corundum in 0.1 and 0.5 m NaCl solutions between 400 and 600 °C from 0.5 to 2.0 kbar. *Geochimica et Cosmochimica Acta*, 65, 2843–2851.
- Wilke, F.D.H., O’Brien, P.J., Altenberger, U., Konrad-Schmolke, M., and Khan, M.A. (2010) Multistage history in different eclogite types from the Pakistan Himalaya and implications for exhumation processes. *Lithos*, 114, 70–85.
- Wirth, R. (2004) Focused Ion Beam (FIB): A novel technology for advanced application of micro- and nanoanalysis in geosciences and applied mineralogy. *European Journal of Mineralogy*, 16, 863–877.
- (2009) Focused Ion Beam (FIB) combined with SEM and TEM: Advanced analytical tools for studies of chemical composition, microstructure and crystal structure in geomaterials on a nanometre scale. *Chemical Geology*, 261, 217–229.
- Zimmermann, R., Heinrich, W., and Franz, G. (1996) Tremolite synthesis from CaCl_2 -bearing aqueous solutions. *European Journal of Mineralogy*, 8, 767–776.

MANUSCRIPT RECEIVED FEBRUARY 2, 2010

MANUSCRIPT ACCEPTED MAY 3, 2010

MANUSCRIPT HANDLED BY EDWARD GHENT